2D MnO$_x$ composite catalysts inspired by natural OEC for efficient catalytic water oxidation

Lizhou Fan,[1][†] Biaobiao Zhang,[1][†][*] Fan Zhang,[2] Brian J.J. Timmer,[1] Oleksandr Kravchenko,[1] Licheng Sun[1,3,4][*]

[1] *Department of Chemistry, KTH Royal Institute of Technology, 10044 Stockholm, Sweden*

[2] *Division of Surface and Corrosion Science, KTH Royal Institute of Technology, Drottning Kristinas väg 51, SE-100 44 Stockholm, Sweden*

[3] *State Key Laboratory of Fine Chemicals, Institute of Artificial Photosynthesis, DUT-KTH Joint Education and Research Center on Molecular Devices, Dalian University of Technology (DUT), 116024 Dalian, China*

[4] *Center of Artificial Photosynthesis for Solar Fuels, School of Science, Westlake University, 310024 Hangzhou, China*

Corresponding author Email: biaobiao@kth.se   lichengs@kth.se

†*These authors contributed equally to this communication.*

Abstract

Birnessite MnO_x is a close inorganic model of natural oxygen-evolving complex (OEC) that has been widely investigated for catalytic water oxidation, yet its activity is limited by the poor active site exposure and sluggish charge transfer. Herein, starting from typical birnessite MnO_x, we fabricated a hybrid of 2D manganese oxide nanosheets and pyridyl modified graphene (MnO_x-NS/py-G) for electrocatalytic water oxidation. Benefiting from the synergy of structural exfoliation, graphene substrate and molecular pyridyl modification, the MnO_x-NS/py-G exhibits abundant catalytically active sites exposure, fast electron transport, and promoted proton transfer at catalyst surface, which imitates the key features of natural OEC. Consequently, the MnO_x-NS/py-G reached over 600 times higher activity compared to the typical birnessite MnO_x. Inspired by nature, this work provides a well-designed and effective strategy to develop highly active manganese oxide-based water oxidation catalysts.

INTRODUCTION

Water oxidation reaction plays an essential role as ideal electron and proton source in artificial photosynthetic strategies, such as hydrogen production, CO_2 reduction, and N_2 reduction. Limited by the multiple proton/electron transfer and high energy barrier, water oxidation suffers from sluggish reaction kinetics and is the bottleneck for most renewable energy systems. Noble metal-based catalysts have been reported as efficient water oxidation catalysts with tolerable activity, yet their scarcity and high cost restrict the large-scale industrialization. One of the biggest challenges in this field is the exploration of cost-effective highly efficient catalysts based on cheap metals.[1-3]

Natural photosynthesis provides a textbook for renewable energy harvesting, in which water oxidation is catalyzed by the oxygen-evolving complex (OEC), a Mn_4CaO_5 cluster, assisted by many functional cofactors for electron and proton transfer (Scheme 1a).[4-6] In addition, manganese possesses a series of advantages, i.e. high natural abundance, low-cost, non-toxicity, and rich redox chemistry for bearing charge accumulation, inspiring the investigation of manganese oxides-based water oxidation catalysts.[7-11] One of the most studied manganese-oxide catalysts is the layered birnessite-type manganese oxide (birnessite MnO_x), which possesses similar structure properties to Mn_4CaO_5 cluster in PSII, e.g., the cubane-like local construction, the mixing of Mn^{3+} and Mn^{4+} oxidation states (Scheme 1b). However, crystalline birnessite MnO_x generally shows moderate water oxidation activity, which is much lower compared with other transition metal-based catalysts. Early studies suggested that the activity of birnessite MnO_x can be influenced by its interlayer ions, interlayer spacing, surface modification and crystallinity.[12-14] Recently, our group fabricated a "c-disordered" birnessite (MnO_x-300) as an efficient water oxidation catalyst.[15-16] Detailed investigation revealed that the partially opened layered structure can facilitate the active site exposure and electron transfer process, which promotes the formation of high-valent Mn^{VII}-oxo active species, improving the activity.[17] These enlightenments suggested that generally applicable strategies to effectively access abundant active sites and fast charge transport need to be explored for the improvement of OER activities of birnessite-type catalysts.
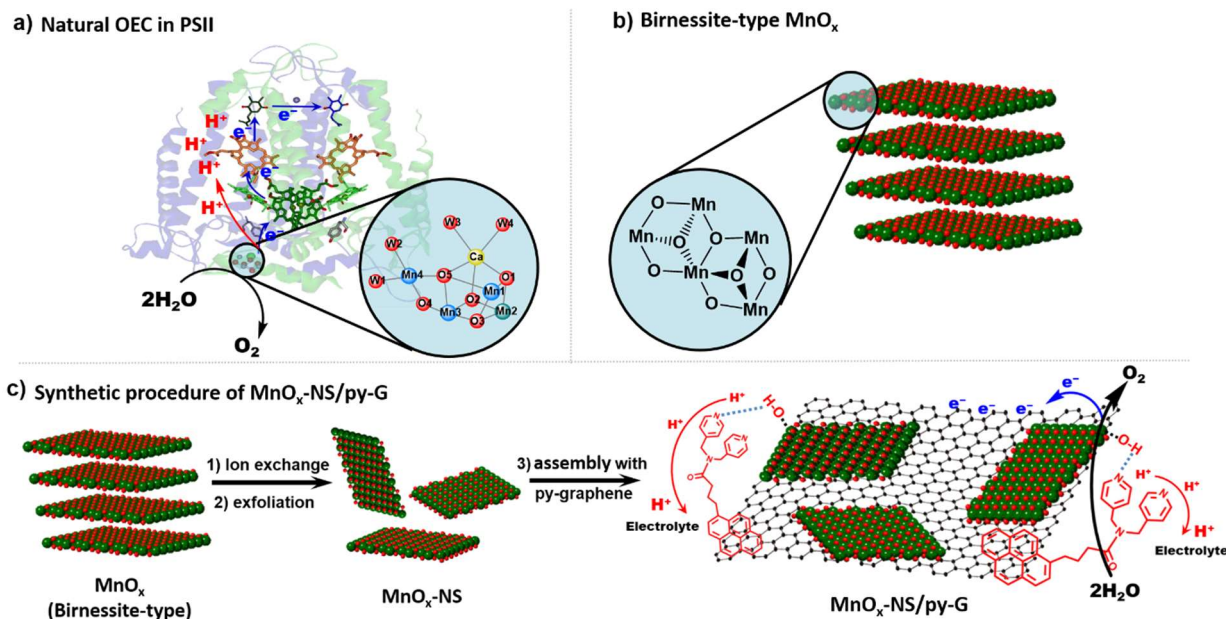
Scheme 1 a) The $CaMn_4O_5$ cluster in PSII of natural photosynthesis. b) The structure of bulk birnessite-type MnO_x. c) Schematic illustration of the MnO_x-NS/py-G and its preparation method.

To acquire sufficient exposure of Mn cubic units, as the Mn_4CaO_5 cluster in PSII, we turned to the structural exfoliation approach (Scheme 1). Two-dimensional (2D) materials have attracted intense attention in recent years owing to several unique properties.[18-19] On one hand, the high aspect ratio in their dimensions can dramatically promote the exposure of coordinatively unsaturated "edge and corner sites" and defects, which have been identified as the highly reactive sites in the δ-MnO_2 catalyst.[20] On the other hand, the high surface energy and unique electronic structure make it feasible to achieve rational modification at the 2D material surface, which can specifically modulate the catalytic kinetics and influence the activity.[21] Inspired by the OEC's well-organized electron and proton transfer channels (Scheme 1a), a combination of exfoliated 2D manganese oxide nanosheets with graphene is further designed to establish a fast electron transportation pathway, and the graphene was in advance modified with a pyridyl molecule to provide a good proton transfer relay for water oxidation by manganese oxides (Scheme 1c),[22-23] synergistically improving the water oxidation activity.

We therefore in this work developed composite water-oxidation catalysts of ultrathin 2D

manganese oxide nanosheets and pyridyl modified graphene (denoted as MnO_x-NS/py-G). By the synergy between structural exfoliation and molecular modification, the MnO_x-NS/py-G achieved 600-fold enhanced catalytic activity compared to bulk birnessite MnO_x. Further in-depth studies indicate that the activity improvement results from the sufficient exposure of catalytically active sites, fast electron transport and efficient proton transfer relay, which arise from adopting the material design inspired by the natural OEC.

RESULTS & DISCUSSIONS

Preparation and Characterization

General synthetic procedures of 2D MnO_x-nanosheet (MnO_x-NS) and MnO_x-NS/py-G are demonstrated in Scheme 1c. A colloidal solution of 2D MnO_x-NS was first obtained from the exfoliation of bulk birnessite MnO_x by an ion-exchange approach, which is shown in the inset of Fig. 1a.[24-26] Typical Tyndall effect is presented on the brown and transparent solution under laser beam illumination, demonstrating its well dispersion and colloidal property. Fig. 1a shows the powder X-ray diffraction (XRD) spectrum of birnessite MnO_x and MnO_x-NS. In contrast to the XRD pattern of birnessite MnO_x with typical sharp peaks, the XRD spectrum of MnO_x-NS presents no distinct diffraction peak. The disappearance of XRD peaks, e.g., the peak at $2\theta =12.4°$ that is related to the layered structure with interlayer spacing of 0.7 nm, illustrates the delamination of long-range ordered layered structure to individual irregularly oriented nanosheets after exfoliation.[24, 26]
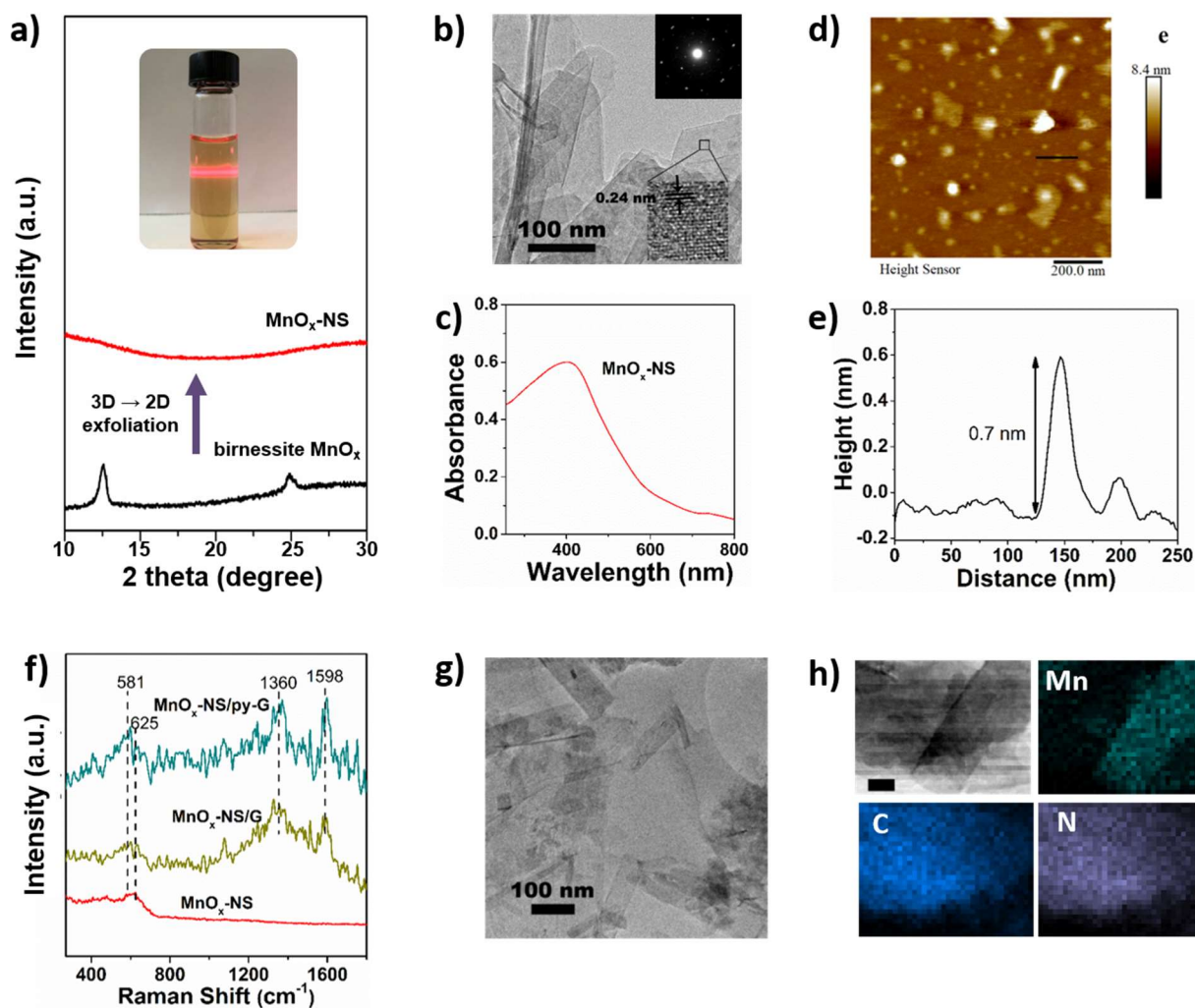
Figure 1 a) Optical image of the colloidal solution of exfoliated MnO_x-NS and XRD pattern of birnessite MnO_x, MnO_x-NS. b) The TEM image of MnO_x-NS. c) The UV-Vis absorption spectra of the colloidal suspension of MnO_x-NS. d) The AFM image and e) Height profile of MnO_x-NS. f) The Raman spectrum of MnO_x-NS, MnO_x-NS/G and MnO_x-NS/py-G. g) The TEM image of MnO_x-NS/py-G. h) STEM-EDX elemental mapping of Mn, C, N of MnO_x-NS/py-G (scale bar is 20 nm).

Transmission electron microscopy (TEM), ultraviolet-visible (UV-Vis) spectroscopy, and atomic force microscopy (AFM) were then conducted to characterize the obtained MnO_x-NS. The TEM image of MnO_x-NS displays a clear single layer nanosheet morphology (Fig. 1b). The selected area electron diffraction (SAED) pattern of MnO_x-NS exhibits hexagonally arranged diffraction spots (inset of Fig. 1b). All these results are in sharp contrast to birnessite MnO_x, which exhibits a multilayered morphology and polycrystal-like SAED image with diffraction rings, showing the

exfoliation of multi-layered structure to monolayer nanosheets (Fig. S3).[26] Notably, both the SAED results of birnessite MnO_x and MnO_x-NS present hexagonal reciprocal lattices, indicating that the MnO_x-NS retains similar crystalline structure as the birnessite MnO_x crystal. The HRTEM image of MnO_x-NS presents lattice fringe with interlayer spacing of 0.24 nm, which can be assigned to the {100} plane of δ-MnO_x.[27-28] The UV-Vis spectrum of MnO_x-NS shows a broad absorption peak around 400 nm, which can be attributed to the *d-d* transition of Mn ions in MnO_6 octahedra (Fig. 1c).[24, 26] At last, the successful exfoliation of birnessite MnO_x to 2D MnO_x monolayer nanosheets was evidently confirmed by AFM imaging of MnO_x-NS (Fig. 1d and e). A thickness of 0.7 nm was determined for the MnO_x-NS, which is close to the thickness of the MnO_x monolayer. [24, 26]

An apparent change in the MnO_x-NS compared to the birnessite MnO_x is the increased ratio of Mn^{3+}/Mn^{4+} oxidation states, which was determined by X-ray photoelectron spectroscopy (XPS). Birnessite MnO_x shows Mn peaks at 643.0, 642.1 eV and 640.7 eV, which can be assigned to Mn^{4+}, Mn^{3+}, and a minimal amount of Mn^{2+} respectively (Fig. S4a).[29-32] Based on the peak integration, its Mn^{3+}/Mn^{4+} content ratio was calculated to be 0.44. Similar Mn 2p XPS peaks were presented for MnO_x-NS. However, the ratio of Mn^{3+}/Mn^{4+} oxidation states increased to 0.67, which is much larger than the 0.44 observed for birnessite MnO_x. Moreover, the ratio of Mn-OH (531.0 eV)/Mn-O-Mn (529.7 eV) is calculated to be 0.46 for MnO_x-NS, much higher than 0.34 of birnessite MnO_x (Fig. S4b).[29-31] These XPS results demonstrate that abundant Mn^{3+} species and coordinatively unsaturated sites are exposed on MnO_x-NS upon 3D → 2D structural exfoliation.

Then, the single layer MnO_x-NS were assembled with graphene and pyridyl modified graphene (py-G), to give the MnO_x-NS/G and MnO_x-NS/py-G samples (Scheme. 1c, see supporting information for details). The Raman spectrum of MnO_x-NS/G and MnO_x-NS/py-G are presented in Fig. 1f. Both the samples show additional scattering bands at 1360 and 1598 cm^{-1} compared with MnO_x-NS, which are the typical Raman signals of graphene.[33-34] The TEM image (Fig. 1g) and energy dispersive spectroscopy (EDS) mapping (Fig. 1h) of MnO_x-NS/py-G display randomly distributed MnO_x-NS on the surface of graphene, without apparent aggregation.

Nitrogen fluorescence signal was evidently presented in the EDS mapping of MnO_x-NS/py-G, confirming the homogeneous modification by the pyridyl molecule. The presence of the pyridyl molecule in MnO_x-NS/py-G can be further depicted by the electrochemical cyclic voltammetry (CV) performance. A broad reduction wave was distinctly presented between -1.0 and -1.35 V (vs Ag/AgCl) for MnO_x-NS/py-G, which is the typical redox peak of pyridine moiety (Fig. S6).[35-36] Overall, these above characterizations thoroughly demonstrate the successful assembly of the MnO_x-NS/py-G composite.

Electrocatalytic water oxidation

Electrocatalytic oxygen evolution reaction (OER) performances of birnessite MnO_x, MnO_x-NS, MnO_x-NS/G and MnO_x-NS/py-G were evaluated by loading on glass carbon (GC) electrodes under alkaline conditions (1 M KOH). Birnessite MnO_x sample shows negligible activity within a wide potential range, which is consistent with the generally low OER activity characteristics of birnessite (Fig. 2a).[12-14] The MnO_x-NS displays significantly enhanced OER activity, which provides approximately 30 times higher current densities compared with that of birnessite MnO_x (Fig. 2a). Notably, after assembling with graphene, the catalytic current density of the MnO_x-NS/G increases a further ten-fold compared to MnO_x-NS (Fig. 2b). Then, with the effect of the pyridyl molecule modification, two times improvement in OER performance was further achieved for the final MnO_x-NS/py-G catalyst compared with MnO_x-NS/G. Added up, in contrast to the initial birnessite MnO_x, the MnO_x-NS/py-G eventually displays 600 times higher OER activity due to structural exfoliation and molecular modification, being ranked as a highly active manganese-based water oxidation catalyst (Fig. S7).
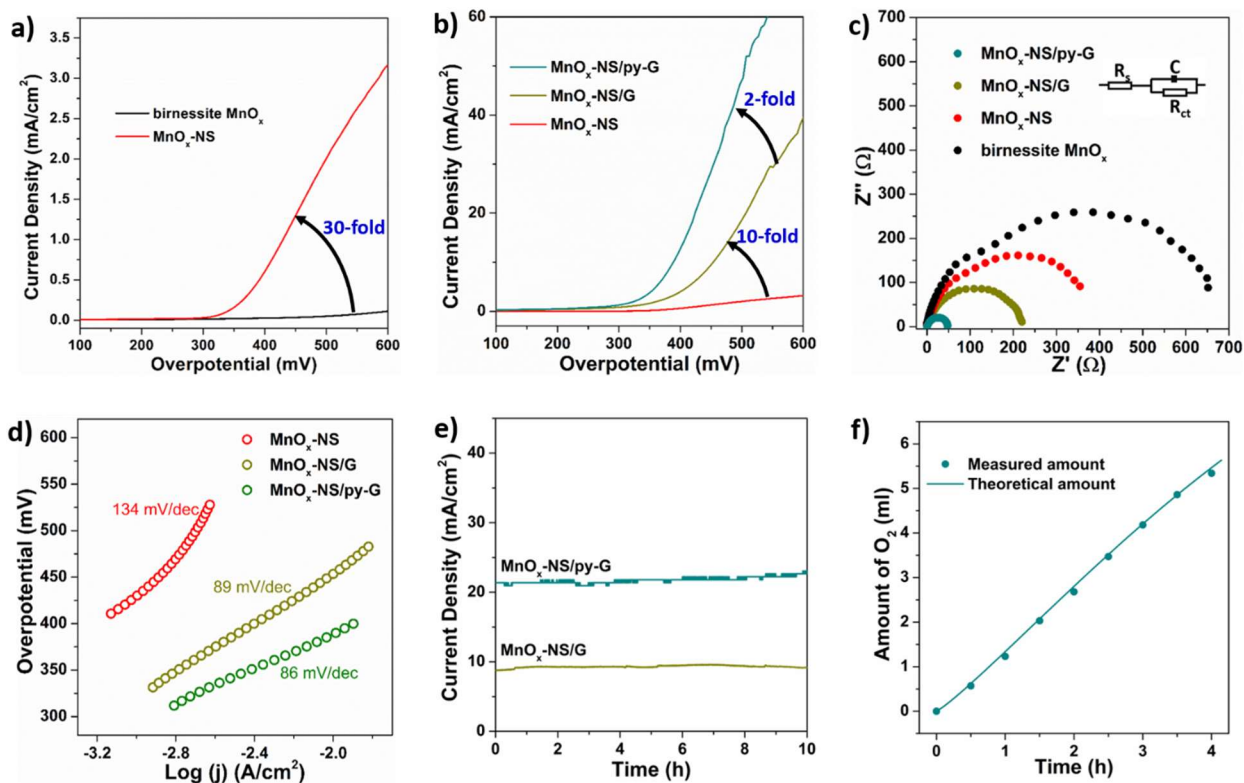
Figure 2 a) Polarization curves of birnessite MnO_x and MnO_x-NS. b) Polarization curves of MnO_x-NS, MnO_x-NS/G and MnO_x-NS/py-G. c) Nyquist diagrams of birnessite MnO_x, MnO_x-NS, MnO_x-NS/G and MnO_x-NS/py-G. d) Tafel slope of MnO_x-NS, MnO_x-NS/G and MnO_x-NS/py-G. e) Chronoamperometry curve of MnO_x-NS/G and MnO_x-NS/py-G under 450mV overpotential. f) The experimental and theoretical O_2 evolution amount by electrolysis of MnO_x-NS/py-G for OER under 400 mV overpotential. Evaluated by loading the catalysts on glass carbon (GC) electrodes under alkaline conditions (1 M KOH).

The improved water oxidation catalysis can be further reflected by the electrochemical impedance spectroscopy (EIS) measurements. The MnO_x-NS/py-G exhibits charge transfer resistance (R_{ct}) of 41.09 Ω, which is 20 times lower compared with 584.8 Ω of the initial birnessite MnO_x (Fig. 2c). A low Tafel slope of 86 mV/dec was determined for the MnO_x-NS/py-G catalyst (Fig. 2d). Chronoamperometric curve was performed on the MnO_x-NS/py-G catalyst to assess the catalytic stability. A stable current density of 21 mA/cm^2 was maintained during 10 h electrolysis under 450 mV overpotential, indicating the excellent electrocatalytic durability of MnO_x-NS/py-G (Fig. 2e). In a separate experiment, the OER Faradaic efficiency was determined to be 98% for MnO_x NS/py-G under 400 mV overpotential

electrolysis, verifying that a vast majority of charges was contributed to water oxidation (Fig. 2f).

Overall, following our design strategy in Scheme 1c, the OER activities of the birnessite MnO_x, MnO_x-NS, MnO_x-NS/G and MnO_x-NS/py-G catalysts have been successively advanced owing to the directed improvement in each sample, achieving the remarkable OER performance for the final MnO_x-NS/py-G. To get insightful understanding on the activity enhancement from the starting inactive birnessite MnO_x to the final active MnO_x-NS/py-G, we then thoroughly examined the specific effects of structural exfoliation, graphene substrate assembly, and pyridyl molecule modification on electrocatalytic water oxidation.

Effects of the structural exfoliation

From birnessite MnO_x to MnO_x-NS, the activity has been increased by 30 times, indicating the significant effects of the structural exfoliation. This dramatic improvement may be induced by two possible ways: i) enlarged electrochemically active surface area (ECSA) caused by morphology change; ii) increased numbers of catalytic sites due to 3D $\rightarrow$ 2D structural changes. To identify effects of the structural exfoliation, we first estimated the ECSA of birnessite MnO_x and MnO_x-NS from their electrochemical double layer capacitance (C_{dl}, Fig. 3a and Fig. S8). The linear slope of MnO_x-NS was calculated to be 0.045 mF/cm^2, which is only 18% higher compared with 0.038 mF/cm^2 of birnessite MnO_x. The similar ECSA of birnessite MnO_x and MnO_x-NS indicates that the layered structure of birnessite MnO_x is already widely accessible for electrochemical charging, which has also been reported on layer double hydroxide materials.[37] Obviously, this slight increase in ECSA cannot account for the 30 times increase in activity upon exfoliation of birnessite MnO_x to MnO_x-NS.

Mn^{3+} species have been commonly recognized as an indicator of active sites for Mn-based water oxidation catalysts.[38-39] To investigate the influence of exfoliation on active sites, pyrophosphate (PP) was introduced to the solution of birnessite MnO_x and MnO_x-NS as a Mn^{3+} trapping agent (Fig. 3b).[16, 39-40] Depicted by the UV-Vis absorption, the MnO_x-NS presents much more Mn^{3+} than birnessite MnO_x, which is consistent with the XPS results, demonstrating the

abundant Mn^{3+} species exposure upon exfoliation. These Mn^{3+} species can positively involve in water oxidation as highly reactive sites, improving the catalytic activity.
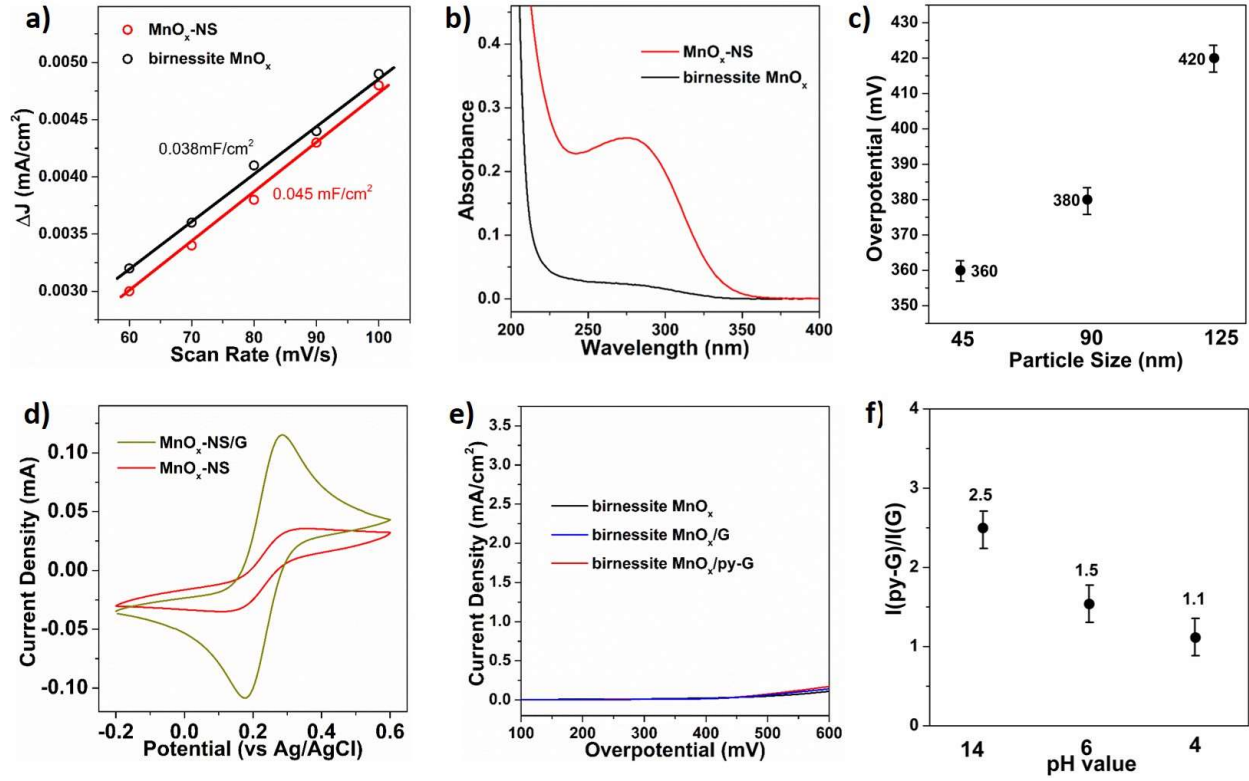

Figure 3 a) The ECSA measurement: ΔJ ($J_a - J_c$) from the CV curves of birnessite MnO_x and MnO_x-NS plotted against scan rates. b) UV−Vis absorption spectra of a 20 mM sodium pyrophosphate solution after dipping of birnessite MnO_x and MnO_x-NS. c) Comparison of the required overpotential for 0.5 mA/cm^2 current density on MnO_x-NS with particle size of 45, 90, and 125 nm. d) CV curves of MnO_x-NS and MnO_x-NS/G in 0.1 M KCl electrolyte containing 10 mM $Fe(CN)_6^{3-/4-}$ ions. e) LSV curves of birnessite MnO_x, birnessite MnO_x/G and birnessite MnO_x/py-G. f) Comparison of I(MnO_x-NS/py-G)/I(MnO_x-NS/G) under pH 14, pH 6 and pH 4 conditions.

Two aspects can result in the effective increase of catalytically active sites by exfoliation. On one hand, the full structural exfoliation can spontaneously promote the active site exposure at the surface of the monolayer nanosheets. To verify this, Na^+ was introduced to MnO_x-NS colloidal suspension to promote the self-reassembly of MnO_x-NS, regenerating layered birnessite MnO_x.[26] The XRD pattern of the re-assembled sample presents typical diffraction peak of layered

structure with interlayer space of 0.73 nm, indicating the reformation of the layered bulk birnessite MnO_x (Fig. S9a). The electrocatalytic performance of this reformed birnessite MnO_x dramatically decreased compared with MnO_x-NS (Fig. S9b). The remarkable activity difference between MnO_x-NS and birnessite MnO_x as well as our previous active "c-disordered" δ-MnO_x demonstrate the importance of surface active site exposure for efficient electrocatalytic water oxidation on δ-MnO_x catalyst.

On the other hand, based on the TEM images, the average particle size of MnO_x-NS was estimated to be around 90 nm (Fig. S10), which is much smaller compared with the 240 nm of birnessite MnO_x. Without the well-ordered layered structure, the MnO_x monolayer collapse and breaks, leading to the decrease in particle size. The formed smaller nanosheets can promote the exposure of coordinatively unsaturated edge- and corner- sites, which are believed to be involved in water oxidation as highly reactive catalytic sites.[37, 41] To further verify, MnO_x-NS with different lateral sizes were separated by controlled centrifugation, denoted as MnO_x-45 and MnO_x-125 (Fig. S11). A close relationship is presented between the lateral size and OER activity: where the MnO_x-45 with smaller particle size shows higher activity than MnO_x-90; whereas the MnO_x-125 with larger particle size displays lower activity compared with MnO_x-90 (Fig. 3c). These results clearly demonstrate the OER activity enhancement with particle size decrement. By the exfoliation process, plenty of coordinated unsaturated edge sites were generated on MnO_x-NS (Fig. S12), which are much easier to be oxidized to essential high valent intermediate states for water oxidation.[15-16, 40, 42-45]

Effects of loading on graphene substrate

The MnO_x-NS/G shows 10 times higher activity compared with MnO_x-NS, indicating the promoting effects of graphene. On one side, the graphene serves as a loading substrate to promote the uniform distribution of MnO_x-NS with less stacking, which has been displayed in the XRD and TEM images of MnO_x-NS/G and MnO_x-NS/py-G (Fig. 1g and S14). More importantly, the graphene substrate with excellent charge transportation capacity can facilitate electron transfer during the OER process.[46-47] To probe the enhancement in electron transfer by graphene, CV was performed in $K_4Fe(CN)_6$ electrolyte (10 mM $Fe(CN)_6^{4-}/Fe(CN)_6^{3-}$) with

MnO$_x$-NS and MnO$_x$-NS/G covered GC electrode as working electrode. In contrast to the broad redox peak of Fe^{2+}/Fe^{3+} for MnO$_x$-NS/GC, a sharp Fe^{2+}/Fe^{3+} peak was observed in the CV curve measured with MnO$_x$-NS/G/GC (Fig. 3d). The promoted Fe^{2+}/Fe^{3+} redox couple on MnO$_x$-NS/G/GC illustrates that the combination of MnO$_x$-NS with graphene effectively solves the slow charge transfer problems. The acceleration of electron transfer can also be demonstrated by the lowered Tafel slopes after graphene introduction (Fig. 2d).[37, 48] The Tafel slopes were calculated to be 89 mV/dec and 86 mV/dec for MnO$_x$-NS/G and MnO$_x$-NS/py-G, which are much smaller than the 134 mV/dec of pristine MnO$_x$-NS, demonstrating the improvement in catalytic kinetics.[16]

Notably, no obvious performance enhancement was observed when the bulk birnessite MnO$_x$ was assembled with graphene or py-graphene, indicating that the promoting effect of graphene requires optimal assembly between graphene and exfoliated 2D nanosheet structure (Fig. 3e). These results demonstrate that the 10-fold enhanced OER activity of MnO$_x$-NS/G compared with MnO$_x$-NS arises from the synergy between graphene loading and 3D → 2D structural exfoliation.

Effects of molecular pyridyl modification

It has been reported that the introduction of pyridine into electrolyte can prominently improve the catalytic performance of MnO$_x$ electrocatalysts[22] and α-Fe$_2$O$_3$ photoanodes.[23] In these systems, the pyridine can work as a proton transfer relay, which facilitates the proton-coupled electron transfer in the catalytic process. For the MnO$_x$-NS/py-G, we directly modified the graphene surface, i.e., the catalytic environment, with a pyridyl molecule to accelerate proton transfer during water oxidation. With this modification, the MnO$_x$-NS loading on graphene afforded a two-fold increase in activity. A pH-dependence of OER activity was established to evaluate the proton transfer property in the catalytic process. Fig. 3f shows the OER activities of the MnO$_x$-NS/G and MnO$_x$ NS/py-G at pH 14, pH 6 and pH 4 electrolyte. In contrast to the significantly enhanced performance under pH 14 and pH 6 conditions, the MnO$_x$-NS/py-G catalyst showed negligible superiority in OER compared with MnO$_x$-NS/G catalyst under pH 4 conditions (see the I(py-G)/I(G) ratio in fig. 3f). The loss of activity enhancement of

MnO_x-NS/py-G under pH 4 can be attributed to the inhibited proton transfer relay effect of the pyridine group, which possesses a pKa value around 5 and is mostly protonated at lower pH. This pH-dependence evidently illustrates the proton transfer relay effect of the modifying pyridyl molecule.[49]

The above thorough analyses elucidate that the origin of the dramatically enhanced catalytic activity of MnO_x-NS/py-G is a combined effect of 3D $\rightarrow$ 2D structural exfoliation, graphene substrate and pyridyl molecule modification. The 2D structure of MnO_x-NS achieved by exfoliation significantly increased the number of catalytically active sites in the MnO_x-NS/py-G catalyst. A synergy between the 2D MnO_x-NS and the graphene substrate provided an efficient electron transfer channel. And the modified proton relay pyridyl molecule promoted proton transfer during water oxidation, accelerating the proton coupled electron transfer (PCET) process.

CONCLUSIONS

In summary, starting from a typical birnessite MnO_x, we obtained a composite MnO_x-NS/py-G by a series of well-designed modifications, including 3D $\rightarrow$ 2D structural exfoliation, graphene assembling, and molecular modification. Resulting from abundant catalytically active site exposure, facilitated electron transport, and efficient proton transfer, the MnO_x-NS/py-G shows remarkably enhanced electrocatalytic water oxidation activity. This work indicates that, to make manganese oxides efficient for electrocatalytic water oxidation, it requires an overall consideration of the full exposure of catalytically active sites and engineered environments for fast electron/proton shuttle, as the team working of OEC in PSII.

CONFLICTS OF INTEREST

The authors declare no competing interest.

ACKNOWLEDGMENT

REFERENCE

1. Han, L.; Dong, S.; Wang, E., Transition-Metal (Co, Ni, and Fe)-Based Electrocatalysts for the Water Oxidation Reaction. *Adv. Mater.* **2016,** *28* (42), 9266-9291.

2. Suen, N. T.; Hung, S. F.; Quan, Q.; Zhang, N.; Xu, Y. J.; Chen, H. M., Electrocatalysis for the Oxygen Evolution Reaction: Recent Development and Future Perspectives. *Chem. Soc. Rev.* **2017,** *46* (2), 337-365.

3. McCrory, C. C.; Jung, S.; Peters, J. C.; Jaramillo, T. F., Benchmarking Heterogeneous Electrocatalysts for the Oxygen Evolution Reaction. *J. Am. Chem. Soc.* **2013,** *135* (45), 16977-16987.

4. Vinyard, D. J.; Ananyev, G. M.; Dismukes, G. C., Photosystem II: the Reaction Center of Oxygenic Photosynthesis. *Annu. Rev. Biochem.* **2013,** *82*, 577-606.

5. Hammarström, L.; Styring, S., Proton-Coupled Electron Transfer of Tyrosines in Photosystem II and Model Systems for Artificial Photosynthesis: the Role of a Redox-Active Link between Catalyst and Photosensitizer. *Energ. Environ. Sci.* **2011,** *4* (7), 2379-2388.

6. Ye, S.; Ding, C.; Chen, R.; Fan, F.; Fu, P.; Yin, H.; Wang, X.; Wang, Z.; Du, P.; Li, C., Mimicking the Key Functions of Photosystem II in Artificial Photosynthesis for Photoelectrocatalytic Water Splitting. *J. Am. Chem. Soc.* **2018,** *140* (9), 3250-3256.

7. Gorlin, Y.; Chung, C. J.; Benck, J. D.; Nordlund, D.; Seitz, L.; Weng, T. C.; Sokaras, D.; Clemens, B. M.; Jaramillo, T. F., Understanding Interactions between Manganese Oxide and Gold that Lead to Enhanced Activity for Electrocatalytic Water Oxidation. *J. Am. Chem. Soc.* **2014,** *136* (13), 4920-4926.

8. Li, A.; Ooka, H.; Bonnet, N.; Hayashi, T.; Sun, Y.; Jiang, Q.; Li, C.; Han, H.; Nakamura, R., Stable Potential Windows for Long-Term Electrocatalysis by Manganese Oxides Under Acidic Conditions. *Angew. Chem. Int. Ed.* **2019,** *58* (15), 5054-5058.

9. Indra, A.; Menezes, P. W.; Zaharieva, I.; Baktash, E.; Pfrommer, J.; Schwarze, M.; Dau, H.; Driess, M., Active Mixed-Valent MnO_x Water Oxidation Catalysts through Partial Oxidation (Corrosion) of Nanostructured MnO Particles. *Angew. Chem. Int. Ed.* **2013,** *52* (50), 13206-13210.

10. Jeong, D.; Jin, K.; Jerng, S. E.; Seo, H.; Kim, D.; Nahm, S. H.; Kim, S. H.; Nam, K. T., Mn_5O_8 Nanoparticles as Efficient Water Oxidation Catalysts at Neutral pH. *ACS Catal.* **2015,** *5* (8), 4624-4628.

11. Kim, J.; Park, S.; Go, Y. K.; Jin, K.; Kim, Y.; Nam, K. T.; Kim, S. H., Probing the Structure and Binding Mode of EDTA on the Surface of Mn_3O_4 Nanoparticles for Water Oxidation by Advanced Electron Paramagnetic Resonance Spectroscopy. *Inorg. Chem.* **2020,** 59 (13) 8846–8854.

12. Thenuwara, A. C.; Cerkez, E. B.; Shumlas, S. L.; Attanayake, N. H.; McKendry, I. G.; Frazer, L.; Borguet, E.; Kang, Q.; Remsing, R. C.; Klein, M. L.; Zdilla, M. J.; Strongin, D. R., Nickel Confined in the Interlayer Region of Birnessite: an Active Electrocatalyst for Water Oxidation. *Angew. Chem. Int. Ed.* **2016,** *55* (35), 10381-10385.

13. Kang, Q.; Vernisse, L.; Remsing, R. C.; Thenuwara, A. C.; Shumlas, S. L.; McKendry, I. G.; Klein, M. L.; Borguet, E.; Zdilla, M. J.; Strongin, D. R., Effect of Interlayer Spacing on the Activity of Layered Manganese Oxide Bilayer Catalysts for the Oxygen Evolution Reaction. *J. Am. Chem. Soc.* **2017,** *139* (5), 1863-1870.

14. Thenuwara, A. C.; Shumlas, S. L.; Attanayake, N. H.; Aulin, Y. V.; McKendry, I. G.; Qiao, Q.; Zhu, Y.; Borguet, E.; Zdilla, M. J.; Strongin, D. R., Intercalation of Cobalt into the Interlayer of Birnessite Improves Oxygen Evolution Catalysis. *ACS Catal.* **2016,** *6* (11), 7739-7743.

15. Zhang, B.; Li, Y.; Valvo, M.; Fan, L.; Daniel, Q.; Zhang, P.; Wang, L.; Sun, L., Electrocatalytic Water Oxidation Promoted by 3D Nanoarchitectured Turbostratic δ-MnO$_x$ on Carbon Nanotubes. *ChemSusChem* **2017,** *10* (22), 4472-4478.

16. Zhang, B.; Chen, H.; Daniel, Q.; Philippe, B.; Yu, F.; Valvo, M.; Li, Y.; Ambre, R. B.; Zhang, P.; Li, F.; Rensmo, H.; Sun, L., Defective and "c-Disordered" Hortensia-like Layered MnO$_x$ as an Efficient Electrocatalyst for Water Oxidation at Neutral pH. *ACS Catal.* **2017,** *7* (9), 6311-6322.

17. Zhang, B.; Daniel, Q.; Fan, L.; Liu, T.; Meng, Q.; Sun, L., Identifying Mn^{VII}-oxo Species during Electrochemical Water Oxidation by Manganese Oxide. *iScience* **2018,** *4*, 144-152.

18. Chhowalla, M.; Liu, Z.; Zhang, H., Two-Dimensional Transition Metal Dichalcogenide (TMD) Nanosheets. *Chem. Soc. Rev.* **2015,** *44* (9), 2584-2586.

19. Tan, C.; Zhang, H., Two-Dimensional Transition Metal Dichalcogenide Nanosheet-based Composites. *Chem. Soc. Rev.* **2015,** *44* (9), 2713-2731.

20. Li, Y. F.; Liu, Z. P., Active Site Revealed for Water Oxidation on Electrochemically Induced delta-MnO$_2$: Role of Spinel-to-Layer Phase Transition. *J. Am. Chem. Soc.* **2018,** *140* (5), 1783-1792.

21. Guo, Y.; Xu, K.; Wu, C.; Zhao, J.; Xie, Y., Surface Chemical-Modification for Engineering the Intrinsic Physical Properties of Inorganic two-Dimensional Nanomaterials. *Chem. Soc. Rev.* **2015,** *44* (3), 637-646.

22. Yamaguchi, A.; Inuzuka, R.; Takashima, T.; Hayashi, T.; Hashimoto, K.; Nakamura, R., Regulating Proton-Coupled Electron Transfer for Efficient Water Splitting by Manganese Oxides at Neutral pH. *Nat. Commun.* **2014,** *5*, 4256.

23. Takashima, T.; Ishikawa, K.; Irie, H., Efficient Oxygen Evolution on Hematite at Neutral pH Enabled by

Proton-Coupled Electron Transfer. *Chem. Commun.* **2016,** *52* (97), 14015-14018.

24. Ma, B.; Hou, W.; Han, Y.; Sun, R.; Liu, Z.-H., Exfoliation Reaction of Birnessite-Type Manganese Oxide by a Host–Guest Electrostatic Repulsion in Aqueous Solution. *Solid State Sci.* **2008,** *10* (2), 141-147.

25. Feng, Q.; Sun, E. H.; Yanagisawa, K.; Yamasaki, N., Synthesis of Birnessite-Type Sodium Manganese Oxides by Solution Reaction and Hydrothermal Methods. *J. Ceram. Soc. Japan*, **1997,** *105* (1223), 564-568.

26. Yang, X.; Makita, Y.; Liu, Z. H.; Sakane, K.; Ooi, K., Structural Characterization of Self-Assembled MnO_2 Nanosheets from Birnessite Manganese Oxide Single Crystals. *Chem. Mater.* **2004,** *16* (26), 5581-5588.

27. Liang, X.; Zhao, Z.; Zhu, M.; Liu, F.; Wang, L.; Yin, H.; Qiu, G.; Cao, F.; Liu, X.; Feng, X., Self-Assembly of Birnessite Nanoflowers by Staged Three-Dimensional Oriented Attachment. *Environ. Sci. Nano* **2017,** *4* (8), 1656-1669.

28. Zhao, G.; Li, J.; Ren, X.; Hu, J.; Hu, W.; Wang, X., Highly Active MnO_2 Nanosheet Synthesis from Graphene Oxide Templates and Their Application in Efficient Oxidative Degradation of Methylene Blue. *RSC Adv.* **2013,** *3* (31), 12909-12914.

29. Wang, H.-Q.; Chen, J.; Hu, S.-J.; Zhang, X.-H.; Fan, X.-P.; Du, J.; Huang, Y.-G.; Li, Q.-Y., Direct Growth of Flower-Like 3D MnO_2 Ultrathin Nanosheets on Carbon Paper as Efficient Cathode Catalyst for Rechargeable Li–O_2 Batteries. *RSC Adv.* **2015,** *5* (89), 72495-72499.

30. Liu, H.; Hu, Z.; Tian, L.; Su, Y.; Ruan, H.; Zhang, L.; Hu, R., Reduced Graphene Oxide Anchored with δ-MnO_2 Nanoscrolls as Anode Materials for Enhanced Li-ion Storage. *Ceram. Int.* **2016,** *42* (12), 13519-13524.

31. Kim, H.; Watthanaphanit, A.; Saito, N., Synthesis of Colloidal MnO_2 with a Sheet-Like Structure by One-Pot Plasma Discharge in Permanganate Aqueous Solution. *RSC Adv.* **2016,** *6* (4), 2826-2834.

32. Zhu, H.; Liu, Q.; Liu, J.; Li, R.; Zhang, H.; Hu, S.; Li, Z., Construction of Porous Hierarchical Manganese Dioxide on Exfoliated Titanium Dioxide Nanosheets as a Novel Electrode for Supercapacitors. *Electrochim. Acta* **2015,** *178*, 758-766.

33. Zabel, J.; Nair, R. R.; Ott, A.; Georgiou, T.; Geim, A. K.; Novoselov, K. S.; Casiraghi, C., Raman Spectroscopy of Graphene and Bilayer under Biaxial Strain: Bubbles and Balloons. *Nano Lett.* **2012,** *12* (2), 617-621.

34. Yan, X. Y.; Tong, X. L.; Zhang, Y. F.; Han, X. D.; Wang, Y. Y.; Jin, G. Q.; Qin, Y.; Guo, X. Y., Cuprous Oxide Nanoparticles Dispersed on Reduced Graphene Oxide as an Efficient Electrocatalyst for Oxygen Reduction Reaction. *Chem. Commun.* **2012,** *48* (13), 1892-1894.

35. Lucio, A. J.; Shaw, S. K., Pyridine and Pyridinium Electrochemistry on Polycrystalline Gold Electrodes and Implications for CO_2 Reduction. *J. Phys. Chem. C* **2015,** *119* (22), 12523-12530.

36. Lebegue, E.; Agullo, J.; Belanger, D., Electrochemical Behavior of Pyridinium and N-Methyl Pyridinium Cations in Aqueous Electrolytes for CO_2 Reduction. *ChemSusChem* **2018,** *11* (1), 219-228.

37. Song, F.; Hu, X., Exfoliation of Layered Double Hydroxides for Enhanced Oxygen Evolution Catalysis. *Nat. Commun.* **2014,** *5*, 4477.

38. Morgan Chan, Z.; Kitchaev, D. A.; Nelson Weker, J.; Schnedermann, C.; Lim, K.; Ceder, G.; Tumas, W.; Toney, M. F.; Nocera, D. G., Electrochemical Trapping of Metastable Mn^{3+} Ions for Activation of MnO_2 Oxygen Evolution Catalysts. *Proc. Natl. Acad. Sci. U.S.A.* **2018,** *115* (23), E5261-E5268.

39. Takashima, T.; Hashimoto, K.; Nakamura, R., Mechanisms of pH-Dependent Activity for Water Oxidation to Molecular Oxygen by MnO_2 Electrocatalysts. *J. Am. Chem. Soc.* **2012,** *134* (3), 1519-1527.

40. Jin, K.; Seo, H.; Hayashi, T.; Balamurugan, M.; Jeong, D.; Go, Y. K.; Hong, J. S.; Cho, K. H.; Kakizaki, H.; Bonnet-Mercier, N.; Kim, M. G.; Kim, S. H.; Nakamura, R.; Nam, K. T., Mechanistic Investigation of Water Oxidation Catalyzed by Uniform, Assembled MnO Nanoparticles. *J. Am. Chem. Soc.* **2017,** *139* (6), 2277-2285.

41. Fan, L.; Zhang, B.; Timmer, B. J. J.; Dharanipragada, N. V. R. A.; Sheng, X.; Tai, C.-W.; Zhang, F.; Liu, T.; Meng, Q.; Inge, A. K.; Sun, L., Promoting the Fe(VI) Active Species Generation by Structural and Electronic Modulation of Efficient Iron Oxide based Water Oxidation Catalyst without Ni or Co. *Nano Energy* **2020,** *72*, 104656.

42. Zhang, B.; Daniel, Q.; Fan, L.; Liu, T.; Meng, Q.; Sun, L., Identifying Mn^{VII}-oxo Species during Electrochemical Water Oxidation by Manganese Oxide. *iScience* **2018,** *4*, 144-152.

43. Zhang, B.; Sun, L., Why Nature Chose the Mn_4CaO_5 Cluster as Water-Splitting Catalyst in Photosystem II: a New Hypothesis for the Mechanism of O-O Bond Formation. *Dalton Trans.* **2018,** *47* (41), 14381-14387.

44. Zahran, Z. N.; Mohamed, E. A.; Naruta, Y., Kinetics and Mechanism of Heterogeneous Water Oxidation by α-Mn_2O_3 Sintered on an FTO Electrode. *ACS Catal.* **2016,** *6* (7), 4470-4476.

45. Mattioli, G.; Zaharieva, I.; Dau, H.; Guidoni, L., Atomistic Texture of Amorphous Manganese Oxides for Electrochemical Water Splitting Revealed by Ab Initio Calculations Combined with X-ray Spectroscopy. *J. Am. Chem. Soc.* **2015,** *137* (32), 10254-10267.

46. Chen, P.; Xu, K.; Zhou, T.; Tong, Y.; Wu, J.; Cheng, H.; Lu, X.; Ding, H.; Wu, C.; Xie, Y., Strong-Coupled Cobalt Borate Nanosheets/Graphene Hybrid as Electrocatalyst for Water Oxidation Under Both Alkaline and

Neutral Conditions. *Angew. Chem. Int. Ed.* **2016,** *55* (7), 2488-2492.

47.   Cui, X.; Ren, P.; Deng, D.; Deng, J.; Bao, X., Single Layer Graphene Encapsulating Non-Precious Metals as High-Performance Electrocatalysts for Water Oxidation. *Energ. Environ. Sci.* **2016,** *9* (1), 123-129.

48.   Vrubel, H.; Moehl, T.; Gratzel, M.; Hu, X., Revealing and Accelerating Slow Electron Transport in Amorphous Molybdenum Sulphide Particles for Hydrogen Evolution Reaction. *Chem. Commun.* **2013,** *49* (79), 8985-7.

49.   Li, W.; Li, F.; Yang, H.; Wu, X.; Zhang, P.; Shan, Y.; Sun, L., A Bio-Inspired Coordination Polymer as Outstanding Water Oxidation Catalyst via Second Coordination Sphere Engineering. *Nat. Commun.* **2019,** *10* (1), 5074.

Graphical Abstract

Natural OEC in PSII

MnO$_x$-NS/py-G

H$^+$

2H$_2$O

O$_2$

Electrolyte

e$^-$ e$^-$ e$^-$

2H$_2$O

Abundant catalytic sites **Fast electron transport** **Mediated proton transfer**